Mechanical Systems and Signal Processing 142 (2020) 106754

Contents lists available at ScienceDirect

Mechanical Systems and Signal Processing

journal homepage: www.elsevier.com/locate/ymssp

An adaptive wavelet packet denoising algorithm for enhanced active acoustic damage detection from wind turbine blades

Christopher Beale, Christopher Niezrecki, Murat Inalpolat *

University of Massachusetts Lowell, 1 University Avenue, Lowell, MA 01854, USA

ARTICLE INFO

Article history:
Received 25 March 2019
Received in revised form 23 January 2020
Accepted 19 February 2020
Available online 28 February 2020

Keywords:
Wavelet packet denoising
Structural health monitoring
Active damage detection
Acoustic
Wind turbine blade

ABSTRACT

The development of a viable structural health monitoring (SHM) technology for the operational condition monitoring of wind turbine blades is of great interest to the wind industry. In order for any SHM technology to achieve the technical readiness and performance required for an operational implementation, advanced signal processing algorithms need to be developed to adaptively remove noise and retain the underlying signals of interest that describe the damage-related information. The wavelet packet transform decomposes a measured time domain signal into a time-frequency representation enabling the removal of noise that may overlap with the signal of interest in time and/or frequency. However, the traditional technique suffers from several assumptions limiting its applicability in an operational SHM environment, where the noise conditions commonly exhibit erratic behavior. Furthermore, an exhaustive number of options exist when selecting the parameters used in the technique with limited guidelines that can help select the most appropriate options for a given application. Appropriately defining the technique tends to be a daunting task resulting in a general avoidance of the approach in the field of SHM.

This work outlines an adaptive wavelet packet denoising algorithm applicable to numerous SHM technologies including acoustics, vibrations, and acoustic emission. The algorithm incorporates a blend of non-traditional approaches for noise estimation, threshold selection, and threshold application to augment the denoising performance of real-time structural health monitoring measurements. Appropriate wavelet packet parameters are selected through a simulation considering the trade-off between signal to noise ratio improvement and amount of signal energy retained. The wavelet parameter simulation can be easily replicated to accommodate any SHM technology where the underlying signal of interest is known, as is the case in most active-based approaches including acoustic and wave-propagation techniques. The finalized adaptive wavelet packet algorithm is applied to a comprehensive dataset demonstrating an active acoustic damage detection approach on a ~46 m wind turbine blade. The quality of the measured data and the damage detection performance obtained from simple spectral filtering is compared with the proposed wavelet packet technique. It is shown that the damage detection performance is enhanced in all but one test case by as much as 60%, and the false detection rate is reduced. The approach and the subsequent results presented in this paper are expected to help enable advancement in the performance of several established SHM technologies and identifies the considered acoustics-based SHM approach as a noteworthy option for wind turbine blade structural health monitoring.

* Corresponding author.
E-mail address: Murat_Inalpolat@uml.edu (M. Inalpolat).

https://doi.org/10.1016/j.ymssp.2020.106754
0888-3270/

1. Introduction

Over the past few decades the global cumulative installed wind capacity has grown at a significant rate, exceeding 500 GW in 2017 [1]. In order to accommodate the substantial growth in wind energy, the size of wind turbine towers and blades increase due to the inverse relationship between the levelized cost of energy and wind turbine size [2,3]. As a result, wind turbine blades are required to endure more challenging operational conditions increasing the frequency of fault events, wind turbine downtime, and overall cost of maintenance [4–6] {Gilman, 2016 #181}. One solution to help reduce the costs incurred from wind turbine blade maintenance would be to implement a condition-based maintenance strategy over the event-based and preventative maintenance strategies currently implemented [7]. A condition-based monitoring system will provide real-time assessment of the blades during operation enabling the ability to identify and track damage as it occurs, curtail or seize wind turbine operation before the damage becomes catastrophic, and schedule maintenance as needed to ultimately reduce overall turbine downtime and cost.

The structural health monitoring (SHM) approach featured in this paper assesses the integrity of cavity structures (e.g. wind turbine blades) by monitoring differences in the acoustic energy transmitted into or out of the structure when subject to damage [8]. Alternative SHM technologies including vibration-based, acoustic emission, thermal, ultrasonic, fiber optic, and photogrammetry have received more attention for wind turbine blade condition monitoring and have performed well in a simulated or laboratory setting [7,9–28]. However, these technologies are generally not well suited for monitoring in the field, largely because of their limited damage detection range in composites requiring a significant number of sensors to cover a large area of interest (e.g. strain gages, piezoelectric and acoustic emission sensors), cost (fiber optic sensors), or effectiveness (accelerometers) [29]. The proposed acoustics-based technique is expected to be unaffected by the aforementioned challenges because the technique is based upon detection of changes in acoustic transmission loss through the cavity structure walls and can be detected by few sensors at large distances from the defect due to the low attenuation of sound in air.

A consistent issue for any SHM technology is measurement noise, and how to remove the noise while retaining the underlying signal of interest [7,27]. Noise becomes more problematic in an operational environment, especially for wind turbines that are exposed to a broad spectrum of environmental noise, such as precipitation and thunder, as well as self-generated noise from aerodynamic loads and the mechanical components of the turbine [30]. Simple spectral filtering is frequently unable to sufficiently remove the noise due to its frequency overlap with the desired signal. In order for any SHM technology to achieve the maturity level and performance required for an operational implementation, advanced signal denoising algorithms need to be established. This work considers the wavelet packet transform (WPT) as a solution to noise removal and signal enhancement.

The WPT decomposes a time domain signal into constituent temporal packets (nodes) pertaining to equal-width frequency sub-bands of the original signal's bandwidth [31,32]. The resultant time-frequency representation allows for the identification of transient events, both desired (damage-induced) and undesired (noise), which may overlap in frequency with the signal of interest. The time-frequency dependent nodal values (wavelet packet coefficients) can be adaptively manipulated to remove undesired noise events and/or used to extract time-frequency damage-based features. Due to the orthogonality of the WPT, the original signal can be perfectly reconstructed from the coefficients obtained from decomposition. The WPT has received considerable attention for denoising data in the fields of image processing, speech processing, audio processing, geophysics and even traffic flow analysis [32–37]. In regards to SHM, wavelets have been studied exhaustively as a damage detection feature with limited consideration to its signal denoising capabilities [38]. This could be due to the limiting assumptions of the traditional algorithm such as pure Gaussian-distributed noise exhibiting constant variance at all frequencies of the measured bandwidth, which is an inappropriate assumption in many operational environments. Furthermore, implementing the algorithm can be intimidating to adapt due to the abundant number of parameters (e.g. wavelet function, decomposition level, threshold selection method, etc...) that can be selected to perform the algorithm with no established method on how to select the most appropriate parameters for a given application [38]. This work applies a replicable simulation to assist in selecting the appropriate parameters and modifies the overall algorithm to accommodate erratic noise environments with non-uniform variance across the bandwidth of interest expected in many operational SHM environments.

In this paper, a novel acoustics-based structural health monitoring approach is extended and significantly improved through the development and application of an adaptive wavelet packet denoising (WPD) algorithm. The WPD algorithm incorporates a blend of non-traditional approaches for noise estimation, threshold selection, and threshold application to augment the denoising performance of real-time SHM measurements. The wavelet parameters are uniquely selected by considering the best trade-off between signal to noise ratio (SNR) improvement and the amount of signal energy retained as determined through an intensive computational simulation. The adaptive WPD algorithm can be easily adopted and optimized through similar simulations by alternative SHM technologies, especially vibration-based and acoustic emission based ones. The finalized algorithm is applied to an experimental database acquired by applying the active acoustic damage detection approach on a 46 m utility-scale wind turbine blade. The wavelet enhanced results are compared with the results obtained from applying simple spectral filters and the overall improvement to the damage detection performance is highlighted.

The paper is structured as follows. The remainder of Section 1 briefly covers the background of the acoustics-based SHM technique and the need for an advanced signal denoising algorithm. Furthermore, the proposed non-traditional modifications to the WPD algorithm are discussed in regards to their purpose and their presence in other studies. In Section 2, the active acoustic damage detection approach is conceptualized. An experimental demonstration of the active approach on a ~ 46 m wind turbine blade from a previous study is summarized to be used later as a candidate set of operational SHM data to verify the efficacy of the adaptive WPD algorithm [39]. The signal processing techniques applied to detect damage in the previous work are also summarized. Section 3 describes the computational steps of the traditional WPD algorithm, followed by the proposed adaptive WPD algorithm that enables denoising in operational SHM environments. Section 4 discusses the procedure and results of the replicable simulation study used to identify the wavelet parameters that yield the best trade-off between improved SNR and retained signal energy. In Section 5, the candidate dataset is conditioned separately using the previously considered high pass spectral filtering approach, and the newly developed adaptive WPD algorithm to compare the damage detection performance improvement. Finally, Section 6 summarizes the potential of the updated acoustics-based SHM technique, the applicability of the adaptive WPD algorithm to operational SHM environments, and the replicability of the simulation study.

1.1. Background in active acoustic damage detection

The acoustics-based SHM technique was first conceptualized by Niezrecki and Inalpolat for wireless damage detection in operational wind turbine blades [8]. The technique is comprised of an active and a passive approach that collaboratively monitor the condition of the structure using a combination of user-generated and naturally generated acoustic excitations measured by externally mounted and cavity-internal microphones. However, only the active acoustic damage detection approach will be considered in this paper. Since its conceptualization, several computational studies have investigated the augmented directivity and transmissibility of acoustic energy from cavity structures exposed to damage and internal acoustic excitation [40–42]. The first experimental investigation of the approach considered a lab-scale wind turbine structure instrumented with a single external microphone on the tower and three wireless Bluetooth speakers, one in each blade [43]. Using simple statistics-based features and a cubic support vector machine learning algorithm, 98% of all damage, consisting of holes and edge splits individually implemented on one of the blades, were detected. Most recently, the active acoustic damage detection approach was applied to a ~46 m wind turbine blade [39]. Damage was detected using differences in the acoustic band power measured by external microphones when compared to an undamaged baseline. The overall damage detection performance was appropriate after manually sifting through the data and removing outliers pertaining to measurements significantly contaminated by noise. However, for the active damage detection approach to be a viable solution for condition-based monitoring of utility-scale wind turbine blades, the computation process needs to be autonomous and the detection performance needs to be significantly enhanced. For this purpose, an adaptive WPD algorithm is developed and applied to the previously acquired data for enhanced damage detection performance with the outcomes presented in this paper.

1.2. Background in wavelet packet denoising

Despite the denoising capabilities of the WPT, the traditional algorithm suffers from several assumptions limiting its performance in many applications, especially when denoising data measured in an operational SHM environment. The modified algorithm developed in this work attempts to mitigate these limitations with the following approaches: node dependent noise estimation, interval dependent threshold application, and SNR dependent threshold selection. Several other studies have attempted similar modifications to the traditional WPD algorithm. Node dependent noise estimation has been used in seismic and speech signal denoising to appropriately model ambient noise characterized by non-uniform variance frequency distributions [44–46]. Interval dependent thresholding has been used in the denoising of gamma ray signals to optimize the thresholds applied to the wavelet coefficients using prior knowledge of the signal of interest's time-frequency structure [46–49]. Lastly, SNR dependent threshold selection has been investigated to enhance the WPD performance of speech signals enabling better estimates of the threshold to be computed based on the signal and noise conditions in real-time [46–48]. In regards to denoising operational SHM data, limited studies have applied WPD in general or considered at least one of the aforementioned modifications. Furthermore, no studies have incorporated all the modifications together in a complementary way and none have identified the parameters using the simulation approach developed in this work [38,50–54].

2. Acoustics-based structural health monitoring

2.1. Active acoustic damage detection approach

The active acoustic damage detection approach, schematically represented in Fig. 1 for a wind turbine blade, targets damage-induced shifts in the acoustic energy transmitted from the internal cavities of the structure to its exterior. Internal acoustic excitations are user-generated by an internal speaker, and the acoustic pressure response in the external air domain

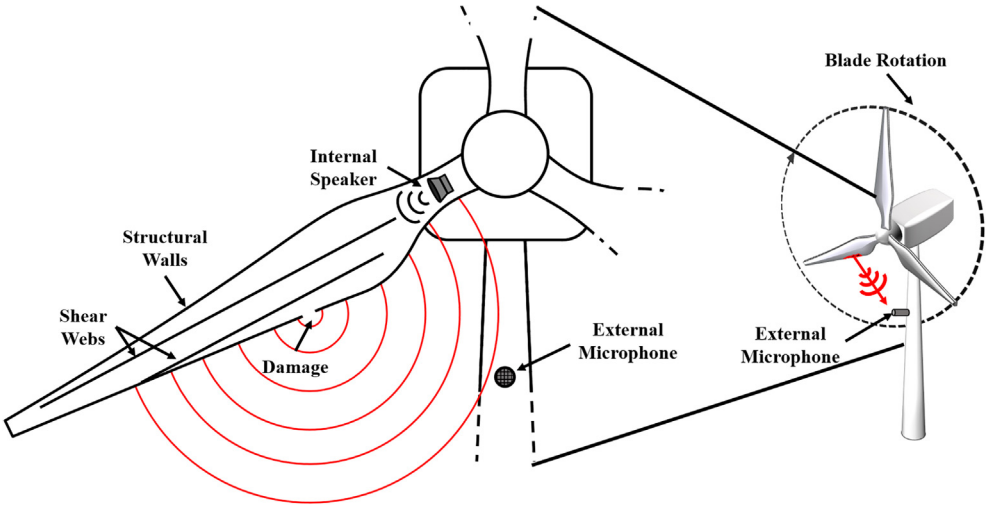

Fig. 1. Schematic of the active acoustic damage detection approach that can be applied to a wind turbine blade.

is measured by a microphone. Over the lifecycle of the structure, damage will occur and progress in severity providing an open-interface between the internal and external air domains of the structure. The damage interface will provide a path for acoustic energy to easily transmit and the damage will manifest itself in the externally measured acoustic pressure responses.

2.2. Active acoustic damage detection data set

The most recently published experimental investigation of the active acoustic damage detection approach was considered in this work for three reasons. First, to enhance the damage detection performance previously acquired. Second, to emphasize the potential of an acoustics-based approach for condition-based monitoring of operational wind turbine blades. Lastly, to serve as a candidate dataset for testing the efficacy of the adaptive WPD algorithm to operational SHM environments. The comprehensive experimental campaign is only briefly summarized to cover the information necessary in this work and complete detail can be found in literature [39].

The active acoustic damage detection approach was demonstrated on a 46 m utility-scale wind turbine blade located at the Wind Technology and Testing Center (WTTC) in Charlestown, Massachusetts. The test matrix, schematically summarized in Fig. 2, included five individually tested damage locations distributed at various distances along the length of the blade (Fig. 2a) [39]. Damage was implemented in the form of cracks or edge splits over six levels of damage severity (Fig. 2b) ranging in length from 0 cm in the undamaged state (D0) to 40.6 cm in the maximum level of damage (D5). Damage was imposed on the blade using an angle grinder with a ~0.2 cm thick blade by grinding the surface until an open interface between the internal cavity and exterior was obtained of the appropriate length. After testing all levels of damage severity, the blade was repaired by sealing the damage interface with 3 M Bondo all-purpose putty.

Two separate hardware configurations were implemented depending on the location of damage and are summarized in Fig. 3. Configuration A (Fig. 3a) was used when damage was implemented before the mid-length of the blade (L1–L3). Two 700 Watt Yamaha CBR10 speakers driven by a Crown XLS 1502 2-channel amplifier were used to acoustically excite the leading edge and trailing edge cavities of the blade. Six microphones were used to acquire acoustic pressure responses consisting of a single microphone internal to the structure (Mic 1) and five external to the structure (Mic 2–6). Microphones 2, 3, and 4 were positioned in-line with the damage at a distance of 3.0 m, 7.6 m, and 15.2 m away from the blade surface, respectively. Microphones 5 and 6 were fixed in position at the mid-length of the blade (~22.9 m down from the root) at a distance of 7.6 m and 15.2 m away from the surface, respectively. Each microphone was equipped with a wind screen and all were PCB model 378A21 random incidence microphones except for Mic 4, which was a PCB model 378B02 free-field microphone.

Configuration B (Fig. 3b) was established after preliminary testing identified issues detecting damage when implemented beyond the mid-length of the blade (L4–L5). It was hypothesized that damage was undetectable due to two major factors. First, two speakers may be unable to sufficiently excite the internal cavities of the voluminous structure when damage was implemented far from the speakers. Therefore, three 700 Watt Yamaha CBR10 speakers driven by a Behringer iNuke NU4-6000 4-channel amplifier were used to acoustically excite all three partially coupled internal cavities of the blade. Second, the improper orientation of the blade, angled 45° up from the horizontal, directed the bulk of the acoustic energy leaking from the damage towards the ground inducing complex acoustic reflections (see Fig. 2a). In order to see if any damage-induced shifts in acoustic transmissibility could be captured, microphones 2, 4, 3, and 6 were repositioned in-line with the damage at shorter distances of 0.3 m, 0.6 m, 3.0 m, and 7.6 m away from the surface, respectively. The positioning of

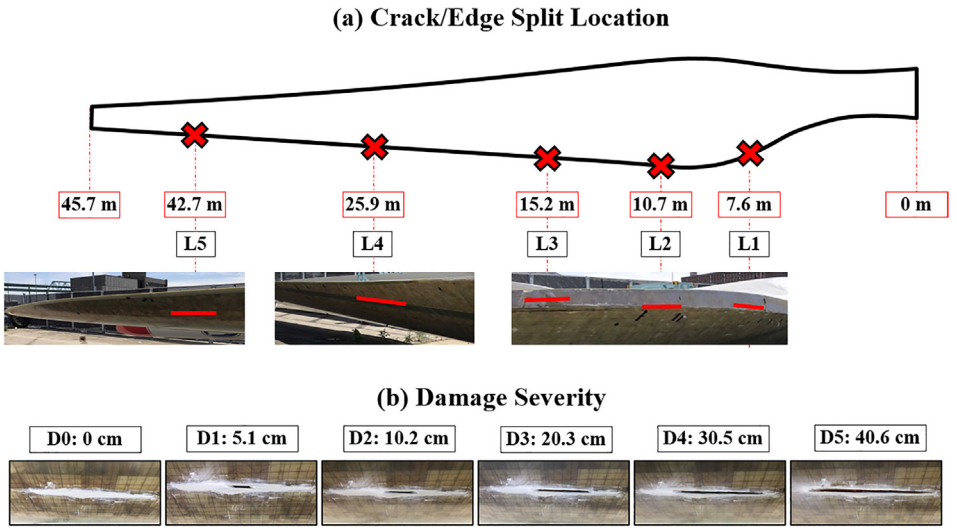

Fig. 2. Schematic of the active acoustic damage detection test matrix demonstrated on the ~46 m blade outlining the (a) location of damage and (b) each individual damage severity level.

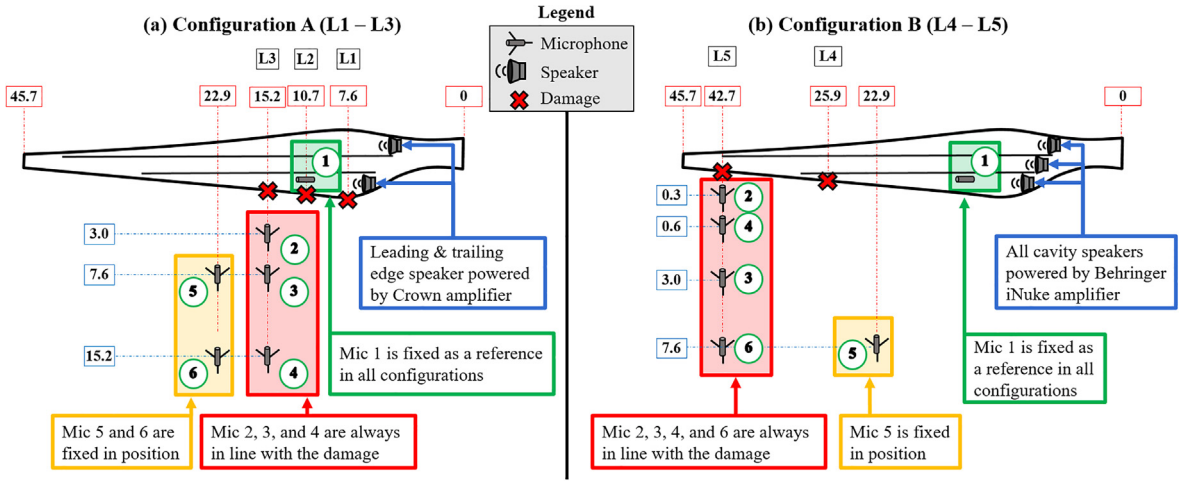

Fig. 3. Schematic of the active acoustic damage detection hardware configurations used when (a) damage was implemented before the mid-length of the blade and when (b) damage was implemented after the mid-length of the blade (All dimensions are in meters).

microphones 1 (internal) and 5 (~22.9 m from the root and 7.6 m from the surface) were unchanged from Configuration A to maintain partial consistency between test cases.

In all tests, data was acquired using an 8-channel m + p VibPilot spectrum analyzer and data acquisition system. A sample rate of 51.2 kHz was used to cover the entire audible spectrum and each measurement block was 131,072 points in length equating to a 2.56 s measurement. In every measurement, the analog output of the VibPilot supplied a linear chirp signal to the amplifier ranging from 0.2 to 20 kHz in frequency over the first 75% of the measurement block (1.92 s). Using a burst chirp signal provided a short period with no excitation allowing proper dissipation of acoustic energy in the internal cavity before the start of the next measurement. For each unique damage location (L1–L5) and each unique damage severity (D0–D5), 150 measurements were acquired to establish a concrete experimental dataset.

2.3. Acoustic damage detection signal processing

The signal processing techniques established to detect damage and distinguish between the different damage states of the blade are based on quantifying the differences between the measured acoustic power spectral density (PSD) estimates and an undamaged baseline. The technique applied in the previous study is replicated in this work with modifications to the

approach taken to remove outliers [39]. All data processing was performed in Matlab® following the procedure schematically depicted in Fig. 4 and briefly summarized as follows [55].

1. The data corresponding to a set of measured acoustic pressure responses from a single microphone, damage location, and damage severity was selected (e.g. all 150 measurements corresponding to the data acquired by Mic 3 during test case L3 at damage level D4).
2. The data was denoised using one of the considered signal conditioning approaches, a high pass spectral filter or the adaptive WPD algorithm, for removing noise contamination and the DC component contained within the data.
3. The acoustic (PSD) was estimated for each of the filtered measurement blocks using Welch's method to assist in reducing spectral leakage and variance using Eq. (1) [56].

$$PSD[f] = \frac{\Delta t}{N}\left|\sum_{n=0}^{N-1} h[n]x[n]e^{-j2\pi fn}\right|^2 \tag{1}$$

In Eq. (1), $PSD[f]$ ($W{\cdot}Hz^{-1}$) is the power spectral density estimate of the f^{th} (Hz) frequency component, $h[n]$ is a window function, and $x[n]$ (Pa) is the time domain signal collected.

4. The acoustic power over larger frequency bands was computed from the PSD estimates to reduce the size of the data considered for detecting damage and the variability amongst individual spectral lines.

$$b[k] = b[f_a, f_b] = \sum_{f=f_a}^{f_b} PSD[f]\Delta f \tag{2}$$

In Eq. (2), $b[k]$ (W) is the average power in thek^{th} frequency band defined by frequencies f_a and f_b, and Δf (Hz) is the frequency resolution.

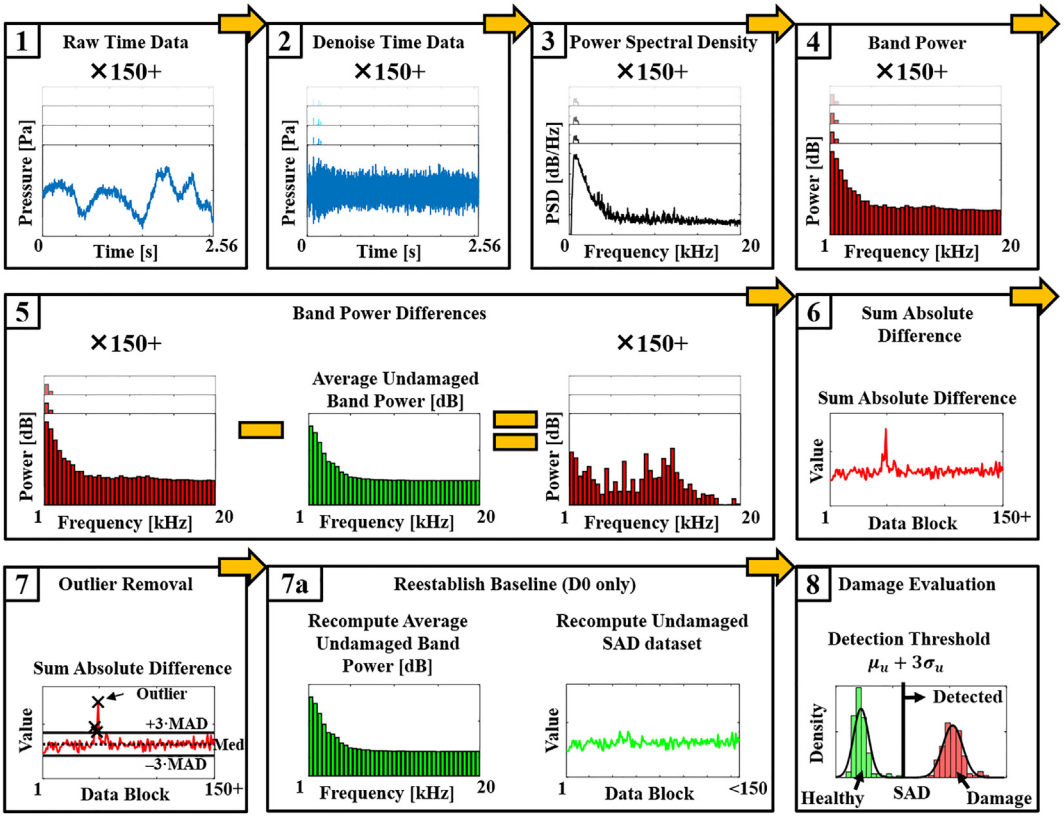

Fig. 4. Schematic depiction of the signal processing procedure used for detecting and distinguishing damage from the experimental database acquired from the active acoustic damage detection demonstration.

5. In order to quantify damage-induced differences in the acoustic transmissibility, the band power estimates were subtracted by an averaged baseline corresponding to the average band power of the undamaged data sub-set measured by the same microphone in the same test case (damage location).

$$\Delta b_d[k] = b_d[k] - \overline{b_u}[k] \tag{3}$$

In Eq. (3), $\Delta b_d[k]$ (W) is the band power difference of the d^{th} damage level (D0, D1...D5), $b_d[k]$ is the band power estimate of the d^{th} damage level and $\overline{b_u}[k]$ is the average band power estimate of the undamaged (D0) data sub-set.

6. The spectral differences were rolled into a single metric for detecting and distinguishing damage, the Sum of Absolute Difference (SAD), simply computed as the sum of the absolute value of the band power differences for each data block.

$$SAD_d = \sum_{k=1}^{K} |\Delta b_d[k]| \tag{4}$$

In Eq. (4), SAD_d is the Sum of Absolute Difference of the d^{th} damage level.

7. An outlier analysis was performed on the SAD values by removing data points corresponding to three median absolute deviations (MAD) above or below the median of the entire dataset.

a.

If the data corresponds to the undamaged level of severity (D0), the average undamaged band power and the SAD were recomputed considering only the measurement blocks retained after removing outliers.

8. The finalized set of processed and outlier-free SAD values were stored for subsequent comparison with the SAD data sub-sets of the same microphone and test location for detecting and distinguishing between the undamaged and damaged states of the blade. A damage detection threshold equal to three standard deviations above the mean of the undamaged data sub-set was established for classifying SAD values that exceeded this threshold as damaged.

The entire eight-step procedure was repeated for each individual set of data corresponding to a unique microphone, damage location, and damage severity starting with the undamaged state (D0). Because all SAD values were computed using the average undamaged band power as a baseline, it was essential to remove outliers in the undamaged set first. As alluded in step eight, only the SAD data sub-sets corresponding to all damage severities (D0–D5) of a single microphone (Mic 2 or Mic3 or etc...) and test case (L1 or L2 or etc...) were compared for evaluation of the damage detection performance. As a result, ambiguity between data acquired on separate days, from separate sensors, under different environmental conditions, and using different test configurations could be avoided.

As previously mentioned, a slight modification was applied to the outlier analysis with respect to the previous work [39]. The previous work considered removing outliers with respect to the individual band power estimates followed by a manual inspection to remove outliers missed by the algorithm. In order to reduce complexity and appropriately evaluate the technique as an autonomous process (optimal for an operational SHM system), the SAD values were considered instead and the manual portion of the outlier analysis was removed. Furthermore, the adaptive WPD algorithm will be more appropriately assessed in regards to how well it can reduce the number of outliers predominantly resulting from noise in the measured data.

3. Wavelet packet denoising

3.1. Wavelet packet denoising concept

The purpose of the WPT is to decompose a measured time response into a series of coefficients that describe its time-frequency structure. The decomposition is performed by correlating the measured response with scaled and shifted wavelet basis functions (waveforms that average to zero and have limited time duration). The resultant coefficients are organized into packets (nodes) corresponding to a specific frequency sub-band related to the scaled wavelets. In each node, the coefficients are temporally ordered based on the shifted position of the scaled wavelets with respect to the measured signal when the correlation was computed. Information can be distinguished at specific frequencies by considering the appropriate node and at specific time intervals by considering the appropriate coefficient indices. Time-frequency localized events, usually representative of the signal of interest or undesired transients, are easily distinguished by large-valued coefficients. Ambient noise, usually exhibiting relatively uniform energy over all time and frequency, results in small-valued coefficients distributed across all the wavelet packet nodes. Therefore, the measured time responses can be denoised by strategically manipulating the coefficients to retain large valued signal-related coefficients, remove large valued transient noise-related coefficients, and threshold small valued ambient noise-related coefficients. The denoised time response is reconstructed by performing the inverse wavelet packet transform (IWPT) on the manipulated coefficients completing the general WPD process.

3.2. Wavelet packet transform computation

Previously mentioned in Section 3.1, the WPT is computed by correlating the measured response with scaled and shifted wavelet basis functions yielding the desired time-frequency dependent wavelet coefficients. However, it is much more computationally efficient and simple to compute the wavelet packet coefficients using a filter-decimation scheme, or filter bank, as illustrated in Fig. 5 [57].

In Fig. 5a, the N-point time domain signal $x[n]$ $(where, n = 1 \cdots N)$ is decomposed into the first level $(j = 1)$ of wavelet packets (nodes) by separately filtering the signal with a low pass scaling filter G and high pass wavelet filter H followed by a downsampling by 2. The resultant $N/2$-point wavelet packet nodes $W_{1,0}$ and $W_{1,1}$ correspond to the temporal information of the original signal in the frequency ranges $[0, f_s/4]$ and $[f_s/4, f_s/2]$, respectively. Finer resolution in the frequency domain is obtained by applying the same filtering and downsampling operations to the wavelet packet coefficients at the previous stage ($W_{1,0}$ and $W_{1,1}$). The result is four $N/4$-point wavelet packets corresponding to the temporal information of the original signal split into four equal-width bands of the Nyquist frequency. The process can be repeated until the desired level is reached or until the length of the wavelet packet coefficients are too low to continue computation. The wavelet packets at the lowest level of the wavelet packet tree ($W_{2,0}$, $W_{2,1}$, $W_{2,2}$ and $W_{2,3}$ in the case of Fig. 5a) are referred to as the terminal nodes. The wavelet packet node that is split and the two wavelet packet nodes that result are referred to as the parent and children nodes, respectively. The original signal is perfectly reconstructed by simply reversing the steps taken to obtain the decomposition, as illustrated in Fig. 5b. The coefficients of a parent node are obtained by adding the coefficients of the children nodes after upsampling by 2 (insert zeros between its values) and filtering with the respective reconstruction filters G' and H'.

It is noted that in Fig. 5, the order of the low pass and high pass filters (G, H, G', and H') were swapped when decomposing and reconstructing node $W_{1,1}$. The swap is required to ensure that the terminal nodes of the WPT are in frequency order, as opposed to natural order [58]. The need for their exchange is a product of the filtering and downsampling operation, and the nodes that require the filter swap to maintain frequency ordering can be determined by a simple two-part rule [57].

3.3. Traditional wavelet packet denoising approach

The actual removal of noise in the WPD process takes place at the terminal nodes after completing the WPT and before performing the IWPT. In order to remove noise in an efficient and simple manner, a broad range of applications have adopted the same or a similar approach to WPD shown schematically in Fig. 6 and summarized as follows [44–46,59,60].

1. The WPT is computed from the measured response to the desired level of decomposition as illustrated in Fig. 5a.
2. An estimation of the noise standard deviation is obtained under the assumptions that the noise is Gaussian distributed and contributes entirely, or dominantly, to the high frequency content of the measured response. An appropriate and robust estimate of the noise standard deviation under these assumptions is obtained by computing the MAD of the high frequency wavelet coefficients in the first level of decomposition, node $W_{1,1}$ [57].

$$\sigma = \frac{median\{|W_{1,1}|\}}{0.6745} \tag{5}$$

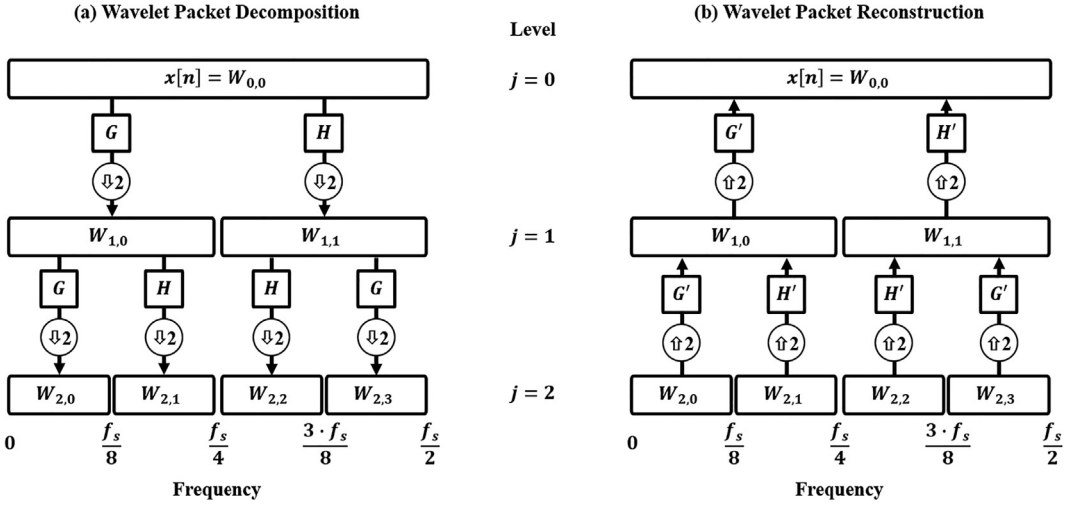

Fig. 5. General filter bank process flow used to recursively (a) decompose the time domain signal into the constituent wavelet packet bases, and (b) reconstruct the time domain signal from the wavelet packet coefficients.

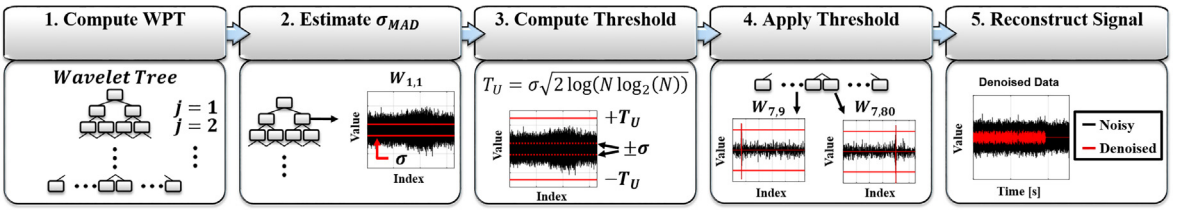

Fig. 6. Traditional wavelet packet denoising algorithm process flow.

In Eq. (5), σ is the standard deviation estimate scaled to a Gaussian distributed random variable. The noise standard deviation is assumed valid for all nodes and frequencies.

3. A threshold value is selected and scaled by the noise standard deviation that represents an appropriate separation between coefficients considered to be noise-related (below the threshold) and signal-related (above the threshold). Although many threshold selection methods exist, the Universal threshold proposed by Donoho and Johnstone is the most common [46,59].

$$T_U = \sigma\sqrt{2\log\left(N\log_2(N)\right)} \tag{6}$$

In Eq. (6), T_U is the Universal threshold which can be shown to equate to or slightly exceed the maximum amplitude of a Gaussian distributed random variable [32].

4. The coefficients are suppressed by applying the threshold to all coefficients of each wavelet packet node. The thresholds can be applied with one of two common approaches, hard or soft. Hard thresholding sets all coefficients below the threshold to zero, and retains all coefficients above the threshold. Soft thresholding similarly sets all coefficients below the threshold to zero, but subtracts the remaining coefficients by the threshold value.
5. The enhanced (denoised) time response is reconstructed by applying the IWPT to the modified coefficients as illustrated in Fig. 5b.

3.4. Adaptive wavelet packet denoising approach

When considering the noise conditions expected in an operational SHM environment, the assumptions established in the traditional WPD approach are no longer valid, rendering the algorithm more or less ineffective depending on the severity of the noise. To accommodate the stringent requirements of an operational SHM environment, significant modifications to the algorithm were established consisting of: (i) node dependent noise estimation, (ii) interval dependent threshold application, and (iii) SNR dependent threshold selection. The purpose of each modification is elaborated in further detail as follows.

3.4.1. Node dependent noise estimation

Traditionally, the WPD approach assumes that the ambient noise is Gaussian distributed with constant variance over the entire bandwidth of the signal and estimates the noise standard deviation from the high frequency wavelet packet coefficients at the first decomposition level ($W_{1,1}$). However, if the ambient noise cannot be entirely characterized with uniform variance across all frequencies (e.g. ocean and wind turbine environments) the noise standard deviation will be inaccurately modeled [30,33,61]. In order to model noise with non-uniform frequency distributions, a frequency dependent noise estimate can be obtained by computing the MAD of each frequency band, or terminal node, separately. Therefore, the threshold of each frequency sub-band (terminal node) will be scaled by the noise standard deviation of the same frequency sub-band. The noise is still assumed to be Gaussian, but with a different variance for each frequency sub-band defined by the terminal nodes as opposed to a single variance for the entire bandwidth defined by the first level high frequency coefficients, which is a more appropriate estimate for the noise environment experienced by wind turbines.

$$\sigma_{L,k} = \frac{median\{|W_{L,k}|\}}{0.6745} \tag{7}$$

In Eq. (7), $\sigma_{L,k}$ is the noise standard deviation of the k^{th} node at the maximum decomposition level, L.

3.4.2. Interval dependent thresholding

In the traditional WPD algorithm, the threshold was applied to all wavelet packet coefficients. This method is appropriate if no information is known about the time-frequency structure of the signal of interest, but exhibits difficulty handling transient events and extraneous noise coefficients that may exceed the threshold. If the time-frequency structure of the underlying signal is known, the wavelet packet coefficients in each node can be partitioned into intervals where only the noise is

known to exist and where the signal and noise are known to exist together. Therefore, the noise-only intervals can be removed entirely mitigating the issue of high amplitude extraneous coefficients and transient events. Furthermore, the noise-only intervals can be used to obtain better estimates of the noise standard deviation using Eq. (7) without any influence from the signal-related coefficients. The time-frequency structure of the signal in this study is known to be a chirp that sweeps linearly from 0.2 kHz to 20 kHz over a 1.92 s time window. Explicit intervals within the time-frequency plane can be defined by computing the wavelet packet transform of the chirp signal and bounding the coefficients that yield non-negligible value. In order to account for reverberation and signal reflections, the bounds were widened by approximately 0.05 s on either side. When considering the experimental data, a time delay corresponding to the time it takes for the source signal to reach the external microphone was applied to appropriately shift and align the bounds with the signal of interest. A snapshot of the signal intervals defined for the source signal can be observed in step 5 of Fig. 7, where the intervals are indicated by the solid red lines and the regions outside the intervals containing noise-only coefficients are faded.

3.4.3. SNR dependent threshold selection

Lastly, the traditional WPD algorithm uses a single threshold selection method that is scaled by the noise estimate to compute the threshold value. Several threshold selection methods exist (Universal, SURE, minimax, etc...) that have varying levels of risk in regards to adversely affecting (suppressing) the signal coefficients. Generally, higher risk thresholds are desired when the signal dominates (high SNR) to obtain good SNR improvements and lower risk thresholds are desired when the noise dominates (low SNR) to ensure lower valued signal coefficients are retained. Thresholding in this manner ensures an appropriate tradeoff exists between SNR improvement and retained signal energy. In the adaptive WPD algorithm, the desired tradeoff between SNR improvement and retained signal energy is maintained by adjusting the risk of the selected threshold based on the SNR of the measured time response. The risk-dependent threshold is computed using Birgé and Massart's adaptive density estimation strategy that determines the best projection of an unknown density from the minimum of a risk function [62,63]. The strategy is easily related and applied to wavelet thresholding, in which the projection of wavelet coefficients that best approximates an unknown signal is determined. Computationally, the threshold value that yields the wavelet coefficients corresponding to the best approximation is determined. The risk function, or penalization criterion, is computed as follows [60,62,63]:

$$risk(t) = -\sum_{k=1}^{t} W_s(k)^2 + 2\sigma_{L,k}t\left(\alpha + \ln\left(\frac{N}{t}\right)\right); t = 1, 2, \cdots, N \tag{8}$$

In Eq. (8), $W_s(k)$ is the absolute value of all wavelet coefficients sorted in descending order, α is the sparsity penalizing term, N is the total number of wavelet coefficients, and t is the current index (number of coefficients in the current subset). It can be observed that the risk function is representative of a trade-off between subsets of the wavelet coefficients and a penalty function that depends on the size of the sample space and the sparsity parameter, α. Increasing or decreasing the

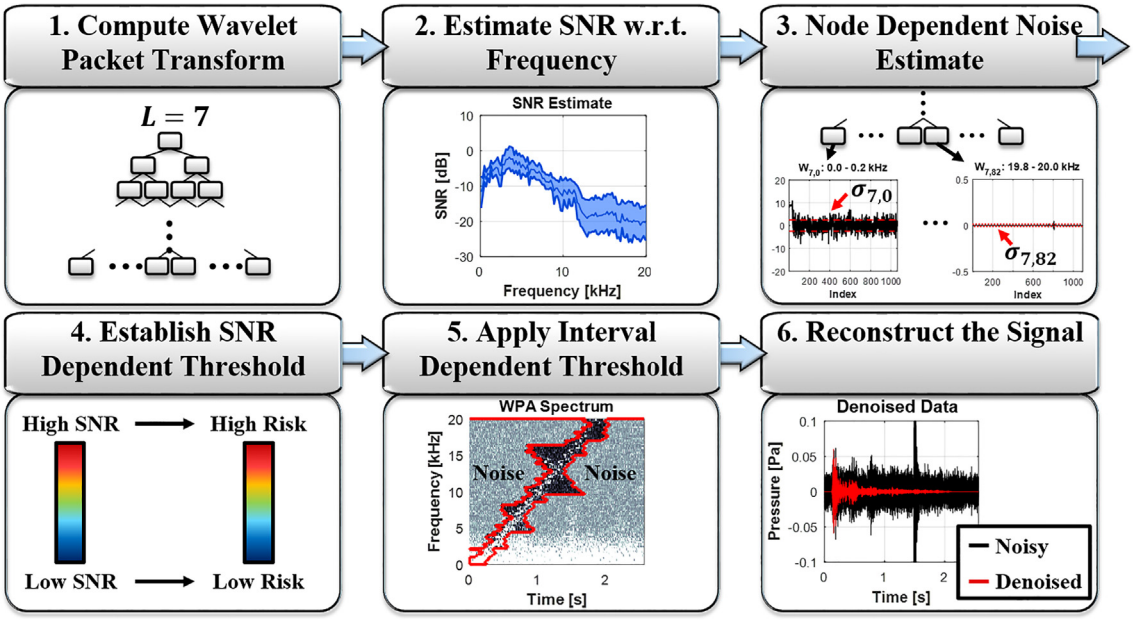

Fig. 7. Adaptive wavelet packet denoising algorithm process flow.

sparsity parameter (risk) will increase or decrease the sparsity of the wavelet coefficients after thresholding, respectively. The index corresponding to the minimum of the risk function, t_{min}, is related to the threshold value that yields the best projection of wavelet coefficients obtained as follows:

$$T_{BM}(\alpha) = W_s(t_{min}) \tag{9}$$

In Eq. (9), $T_{BM}(\alpha)$, is the threshold value obtained from the Birgé-Massart strategy for a given value of α. In the adaptive WPD algorithm, the sparsity parameter is adjusted with respect to the estimate of the SNR for each measurement to maintain the appropriate tradeoff between SNR improvement and retained signal energy. Furthermore, the SNR is recomputed for each successive measurement to appropriately account for fluctuations in the behavior of the noise environment. The SNR is computed for each individual node to obtain a frequency dependent estimate as follows.

$$SNR_k = 10\log_{10}\left(\left|\frac{RMS(W_{L,k})^2 - RMS(W_{L,k,n})^2}{RMS(W_{L,k,n})^2}\right|\right) \tag{10}$$

In Eq. (10), SNR_k is the signal to noise ratio corresponding to the frequency sub-band of the wavelet packet node $W_{L,k}$, and $W_{L,k,n}$ are the coefficients corresponding to the noise-only interval of the wavelet packet node $W_{L,k}$.

3.4.4. Adaptive wavelet packet denoising algorithm

Considering all modifications, the entire adaptive WPD algorithm is outlined schematically in Fig. 7 and summarized as follows.

1. The WPT is computed from the measured response to the desired level of decomposition as illustrated in Fig. 5a.
2. The SNR is estimated with respect to frequency by computing Equation (10) for each terminal node.
3. The noise standard deviation is computed using Equation (7) for each terminal node only considering the coefficients in the noise-only interval.
4. The threshold value is computed for each terminal node using Eqs. (8) and (9) and the appropriate sparsity parameter a, selected based on the results obtained in the adjusted according to the SNR computed in step 2. The relationship between α and the estimated SNR was obtained from the numerical simulation study and is presented in Section 4.4.4
5. The coefficients corresponding to the noise-only intervals are set to 0 for each terminal node and the remaining coefficients (signal and noise) are suppressed by the respective threshold values computed in step 4.
6. The enhanced (denoised) time response is reconstructed by applying the IWPT to the modified coefficients as illustrated in Fig. 5b.

4. Wavelet packet parameter simulation study

The ultimate goal of the WPT is to obtain the sparsest representation of wavelet coefficients where a few large coefficients exist that describe the signal of interest while all remaining coefficients are small and describe the noise. In this representation, the signal is easily distinguished from noise and thresholding can be performed with minimal risk (loss of small-valued signal-related coefficients). However, the WPT can be applied using an abundant number of parameters that can be modified to yield different representations of the wavelet coefficients all describing the same measured response. In order to determine the ideal wavelet parameters, a simulation study was performed considering each wavelet parameter's influence on the tradeoff between improved SNR and retained signal energy. Performing the simulation in this manner enables the parameters to be selected that best benefit the performance of signal denoising for operational SHM purposes. The following sub-sections outline the simulation study as applied to the active acoustic damage detection tests described in Section 2.2, and can be easily applied for other SHM applications.

4.1. Wavelet parameters

The wavelet parameters considered to have a substantial influence on the WPD algorithm performance are the following: the wavelet function used in the WPT, the level of decomposition considered, the threshold selected for suppressing the coefficients (value of the sparsity parameter, α), and the method applied to threshold the coefficients (hard or soft). The effectiveness of each parameter will depend on the shape and time-frequency structure of the signal of interest, the severity of noise, and the ultimate goal of denoising (e.g. signal quality improvement in speech processing versus SNR improvement in signal denoising). This work considers a total of 23 wavelet functions, 10 decomposition level, 10 thresholds, and 2 threshold application methods summarized in Table 1. However, different variations of the same parameters could be included for any desired application. In total, simulating all the considered parameters would make 4600 different combinations. In actuality, the number of combinations simulated was less as optimal parameters were identified and less appropriate parameters ruled out.

Table 1
Summary of wavelet parameters considered in the simulation study. (O corresponds to the wavelet filter order).

Parameter	Simulated Options		Total
Wavelet Function	*DaubechiesO* (*dbO*) :	$O = 1, 5, 10, 15, 20, 25, 30, 35, 40, 45$	23
	SymletsO (*symO*) :	$O = 5, 10, 15, 20, 25, 30, 35$	
	CoifletsO (*coifO*) :	$O = 1, 3, 5$	
	Fejer − Korovkin O (*fkO*) :	$O = 4, 14, 22$	
	DiscreteMeyer (*dmey*) :	*NotApplicable*	
Decomposition Level	L :	$L = 1, 2, 3, 4, 5, 6, 7, 8, 9, 10$	10
Threshold Selection	$T_{BM}(\alpha)$:	$\alpha = 1, 2, 3, 4, 5, 6, 7, 8, 9, 10$	10
Threshold Application	*Method* :	*Hard*, *Soft*	2

4.2. Quality assessment metrics

The effectiveness of each wavelet parameter on the denoising performance was evaluated by three quality assessment metrics: the SNR improvement, the percentage of energy retained after denoising considering solely the signal of interest, and the entropy of the wavelet coefficients. Each of the three metrics were selected specifically to quantify how well the approximation preserved the clean signals energy (percent energy retained) and how much the approximation enhanced the distinguishability of the clean signal from the noise (SNR improvement and entropy). As implied by the signal processing techniques outlined in Section 2.3, the active damage detection approach relies on quantifying the spectral magnitudes estimated from external acoustic pressure responses. The ability to accurately quantify the spectral magnitudes in the presence of noise is essential to the damage detection performance of the acoustics-based technique, which is also essential for many other SHM techniques such as acoustic emission and vibration based techniques.

4.2.1. Signal to noise ratio improvement

The SNR is defined as a ratio between the signal of interest power and the noise power. In order to quantify the SNR improvement, the SNR after applying the WPD algorithm must be quantified. It is common to estimate this posterior SNR by using the original clean signal as the signal power or the residual noise after denoising as the noise power [50,54,64,65]. However, this is not entirely true due to the inevitability that the smaller signal-related coefficients (below the threshold) will be removed. Therefore, the actual amount of clean signal power after denoising may be less than the original clean signal power and the residual noise may contain a portion of the original clean signal or exclude noise that was missed during the WPD process (e.g. noise coefficients that were above the threshold). In order to accurately estimate the posterior SNR, the WPD process was applied to the clean signal without any added noise using the thresholds established from the clean signal with added noise. The resultant reconstructed response corresponds solely to the signal content retained from the WPD process, labeled the denoised clean signal. Furthermore, the denoised clean signal was subtracted from the reconstructed response obtained by applying the WPD process to the clean signal with added noise to obtain the noise-content remaining after denoising. Now the SNR improvement can be appropriately calculated as follows:

$$\Delta SNR = SNR_P - SNR_I = 10\log_{10}\left(\frac{RMS(x_{sd})^2}{RMS(x_d - x_{sd})^2}\right) - 10\log_{10}\left(\frac{RMS(x_s)^2}{RMS(x_n)^2}\right) \tag{11}$$

In Eq. (10), ΔSNR is the SNR improvement, SNR_P is the posterior SNR, SNR_I is the initial SNR, x_{sd} is the denoised response without added noise, x_d is the denoised response with added noise, x_s is the signal of interest, and x_n is the noise. Larger values of ΔSNR correspond to better denoising performance.

4.2.2. L_2R ratio

The percentage of energy retained corresponding solely to the signal of interest was computed as a ratio between the *l-2* norm of the denoised response without added noise and the original signal of interest.

$$L_2R = \frac{\Sigma_{n=1}^{N}|x_{sd}[n]|^2}{\Sigma_{n=1}^{N}|x_s[n]|^2} \tag{12}$$

In Eq. (12), L_2R is the *l-2* norm ratio. The ideal value of L_2R is unity, implying that no energy was lost during the WPD process. Careful inspection of the ΔSNR and L_2R is required to ensure that the desired tradeoff between noise removed and energy preserved is maintained.

4.2.3. Entropy

Entropy serves as a metric for quantifying the disorder of the wavelet packet coefficients (how evenly/unevenly distributed the values are), and can be computed as follows [66].

$$Q_{j,k} = -\Sigma_t^{T_j} W_{j,k}^2(t)\log_2\left(W_{j,k}^2(t)\right) \tag{13}$$

In Eq. (13), $Q_{j,k}$ is the entropy of the k^{th} node at the j^{th} level, t corresponds to the coefficient index of the wavelet packet node, and T_j is the number of coefficients in the wavelet packet nodes at the j^{th} level. The entropy will be large when the value of coefficients is evenly distributed, and small when large values coincide with few coefficients. Smaller values of entropy are desired corresponding to fewer large valued signal coefficients, enhancing the ability to distinguish the signal of interest and transient noise events from the ambient noise.

4.3. Simulation process flow

The simulation was performed considering the same acoustic excitation signal used in the active damage detection approach (a 2.56 s, 75% burst chirp from 0.2 kHz to 20 kHz) described in Section 2.2 as the signal of interest. The signal of interest can be easily adjusted based on the desired application. The initial SNR conditions ranged from −12 dB to 12 dB in steps of 1 dB and were generated by superimposing the Gaussian distributed noise to the signal of interest. The entire computational simulation is outlined schematically in Fig. 8 and summarized as follows. The procedure was repeated until all desired parameter combinations were evaluated.

1. The clean signal of interest is generated and superimposed with noise to the desired initial SNR.
2. A wavelet function is selected for the WPT.
3. The WPT is computed using the selected wavelet function to the desired level of decomposition.
4. All considered thresholds are computed corresponding to the desired risks (α).
5. The threshold is applied to the wavelet packet coefficients using the desired threshold application method.
6. The three quality assessment metrics are computed from the reconstructed response.

4.4. Simulation results

4.4.1. Threshold application method

Hard thresholding was selected as the appropriate threshold application method for the adaptive WPD algorithm because it best preserved the signal energy. Fig. 9 compares the time response (Fig. 9a) and PSD estimates (Fig. 9b) obtained by denoising with hard and soft thresholding against the original clean simulated chirp signal. The chirp signal that was denoised had a SNR of 0 dB and the WPD process was performed with a decomposition level of 7, dmey wavelet function, and the $T_{BM}(5)$ threshold. Inspecting Fig. 9, it is easily observed that the amplitude of the time response obtained when hard thresholding was used closely matches the amplitude of the clean signal. Similarly, the magnitude of the PSD obtained from hard thresholding closely matches the clean signal as shown in Fig. 9b. On the other hand, the amplitude of the time response and magnitude of the PSD obtained from soft thresholding is generally less than the clean signal. In Section 3.3, soft thresholding was defined to subtract all coefficients above the threshold by the threshold value. The coefficients above the threshold ideally (and in most cases) correspond to the signal-related coefficients and their suppression results in signal energy attenuation as observed in Fig. 9. The reason soft thresholding has received interest resides in its ability to preserve signal regularity, which is beneficial for enhancing audio or speech signals. In the case of denoising data in an operational SHM environment, energy preservation is critical and hard thresholding is required.

4.4.2. Level of decomposition

The selected level of decomposition was determined by comparing the tradeoff between the SNR improvement (ΔSNR) and signal energy preserved (L_2R). In this work, it was desired to preserve most of the signal energy due to the dependency

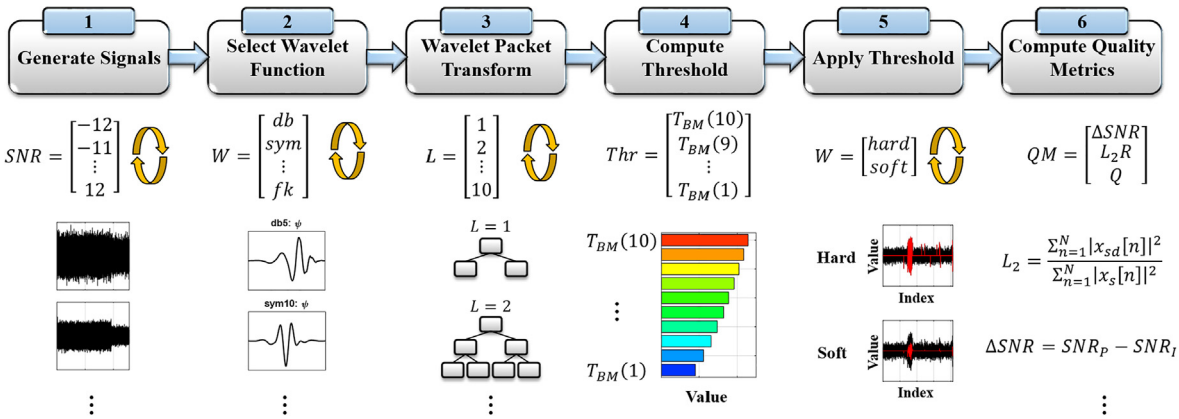

Fig. 8. General computational simulation process flow performed to evaluate the efficiency of the desired wavelet parameters.

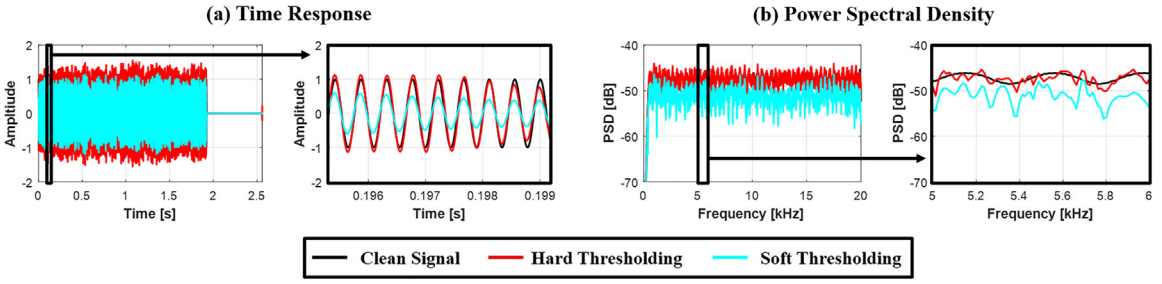

Fig. 9. (a) Time response of the clean simulated chirp, and the resultant responses obtained from denoising the simulated chirp with different thresholding approaches when contaminated with noise at an SNR of 0 dB using a level 7 WPT, dmey wavelet function, and $T_{BM}(5)$ threshold, and (b) the power spectral density estimates corresponding to each of the time responses.

of accurately quantifying the spectral magnitudes. Therefore, a minimal limit of $L_2R \geq 0.9$ was established. This limit can be adjusted to consider preserving more or less than at least 90% of the signal energy depending on how essential energy preservation is for the desired application. Fig. 10 shows a heatmap of the ΔSNR obtained using the WPD algorithm with a db35 (Daubechies wavelet 35) wavelet function for three thresholds corresponding to a high (Fig. 10a), moderate (Fig. 10b), and low risk (Fig. 10c). The conditions of initial SNR and decomposition level that yielded a $L_2R < 0.9$ are washed out to easily distinguish the appropriate conditions that satisfy the desired L_2R conditions. Regardless of the severity of thresholding risk, the level of decomposition that could preserve at least 90% of the signal energy at the lowest SNR was consistently level 7. Furthermore, the largest ΔSNR for all applicable ($L_2R \geq 0.9$) initial SNR conditions was obtained using a decomposition level of 7. Similar conclusions were observed even when reviewing the results obtained by applying the other considered wavelet functions and thresholds. This is true because the time-frequency structure of the chirp signal is the same regardless of the other parameters and was described best by the time-frequency resolution corresponding to a decomposition level of 7.

4.4.3. Wavelet function

The wavelet function was selected based on all three quality metrics using the selected decomposition level of 7. Considering the entropy, Fig. 11 shows a heatmap of the average nodal entropy with respect to the initial SNR of the signal and the wavelet function used in the WPT. Each row of the heatmap is scaled such that the wavelet functions yielding the lowest entropy could be easily identified regardless of the initial SNR (shading that corresponds to 0 in the color bar). In Fig. 11, the average nodal entropy at an initial SNR of 6 dB was extracted and ordered from worst to best showing select examples of the $W_{7,62}$ coefficients and the wavelet function used to compute them. It can be observed how the wavelet coefficients become increasingly sparse as the entropy decreases. Furthermore, the shape and regularity of the wavelet function aligns with that of a chirp function as the entropy decreases and the filter order increases.

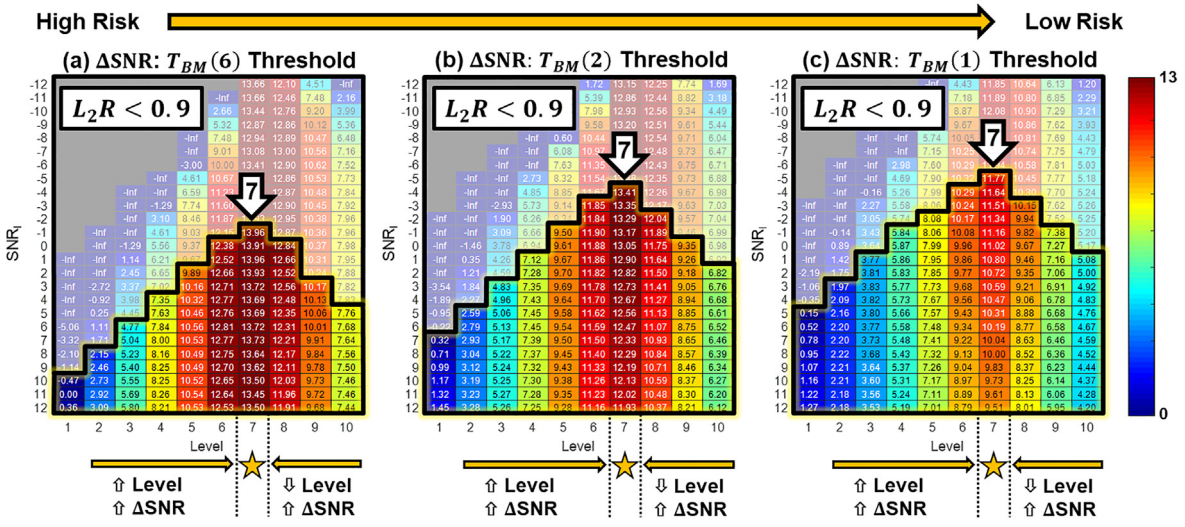

Fig. 10. Heatmap of SNR improvement highlighting parameter combinations that yielded an $L_2R \geq 0.9$ when WPD was performed with a db35 wavelet function using a (a) $T_{BM}(6)$ threshold (high risk), (b) $T_{BM}(2)$ threshold (moderate risk), and (c) $T_{BM}(1)$ threshold (low risk).

In order to select a wavelet function appropriate for the denoising application under consideration, the wavelet functions were ranked based on the number of occurrences in which they were amongst the five wavelets yielding the largest L_2R, largest ΔSNR, and lowest entropy for each initial SNR. The top five and last wavelets are ranked and tabulated in Table 2. Although the dmey wavelet function is consistently one of the best in terms of L_2R and ΔSNR, it doesn't appear at all within the top five wavelets for entropy. The wavelet function that consistently appears in the top five wavelets for all quality metrics is the db35 wavelet. Therefore, the db35 was selected for the adaptive WPD algorithm.

4.4.4. SNR-dependent threshold selection limits

In order to determine the appropriate threshold yielding the desired tradeoff between energy preserved and noise removed with respect to initial SNR, a heatmap of the ΔSNR was analyzed, and is shown in Fig. 12. The results in Fig. 12 were obtained by applying the wavelet function (db35), level of decomposition (7), and thresholding application method (hard) selected as the most appropriate in sections 4.4.1–4.4.3. The parameters that yielded a $L_2R < 0.9$ are faded out and all but the parameters yielding the best ΔSNR are grayed out in the heatmap. The intervals in which each threshold selection method yields the best ΔSNR were extracted from the ΔSNR heatmap and employed in the adaptive WPD algorithm. Specifically, $T_{BM}(1)$ yields the best SNR improvements when the initial SNR is between $[\infty, -4]$ dB, $T_{BM}(2)$ is best between $[-4, -3]$ dB, $T_{BM}(3)$ is best between $[-3, -2]$ dB, $T_{BM}(4)$ is best between $[-2, 0]$ dB, and $T_{BM}(5)$ is best between $[0, \infty]$ dB.

The intervals extracted from Fig. 12 correspond to the threshold selection method that should be used, given the initial SNR is correct. However, the SNR is estimated from measured data and will exhibit uncertainty. The uncertainty was quantified during the simulation by subtracting the estimated SNR by the known initial SNR. The average error bounded by a standard deviation was computed and is shown in Fig. 12. The limits extracted from the ΔSNR heatmap were modified by adding the standard deviation value corresponding to the appropriate SNR.

Note that the interval in Fig. 12 corresponding to the lowest risk threshold (A1) extends beyond the lowest initial SNR (-5 dB) that satisfies the desired L_2R limit of $L_2R \geq 0.9$. Intuitively it makes sense to reject the response when the signal is dramatically contaminated with noise, which would correspond to setting all coefficients of the wavelet nodes exhibiting lower SNRs to zero. Several issues arise from applying such a dramatic threshold. First, suppressing the coefficients entirely would preserve none of the signal energy over the corresponding frequency sub-bands which is counterintuitive to the ultimate

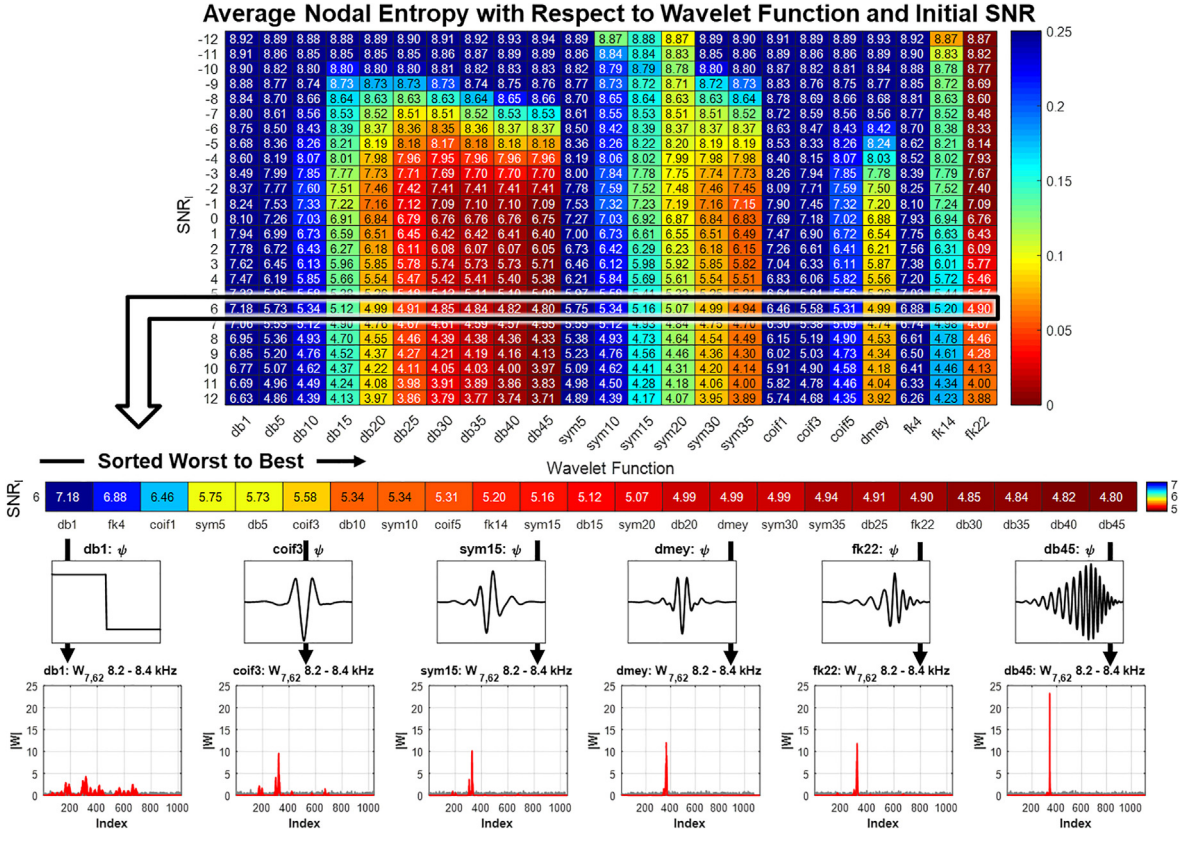

Fig. 11. Heatmap of the average nodal entropy from the WPT computed to a decomposition level of 7 with respect to initial SNR and wavelet function used. The average nodal entropy values corresponding to an initial SNR of 6 dB are extracted and ordered from worst to best showing select examples of the $W_{7,82}$ coefficients and the wavelet function used to compute them.

Table 2
Wavelet functions ranked by the number of occurrences in which they were amongst the five wavelets yielding the largest L_2R, largest ΔSNR, and lowest entropy for each initial SNR.

Order	*L2R*		*ΔSNR*		*Entropy*	
	Wavelet	Frequency	Wavelet	Frequency	Wavelet	Frequency
1	dmey	23	sym35	23	db30	20
2	sym30	22	dmey	22	**db35**	19
3	sym35	22	sym30	21	fk22	19
4	**db35**	14	db40	16	db45	18
5	db40	14	**db35**	12	db40	16
⋮	⋮	⋮	⋮	⋮	⋮	⋮
Last	db1	0	db1	0	db1	0

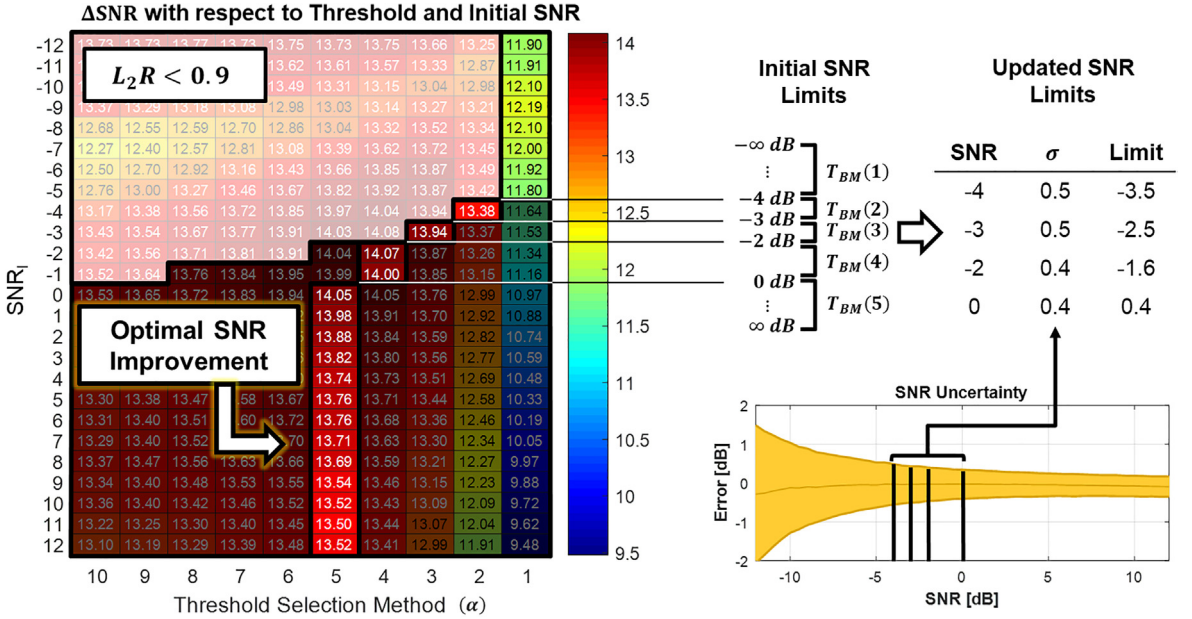

Fig. 12. Heatmap of the ΔSNR with respect to initial SNR and threshold selection method applying the WPD algorithm with a db35 wavelet, decomposition level of 7, and hard thresholding. The average error of the SNR estimates bounded by a single standard deviation is shown with respect to the initial SNR. The standard deviations extracted from the SNR uncertainty plot are added to the initial SNR limits to obtain the updated SNR limits.

goal of the denoising process. Secondly, thresholding the response in such a dramatic manner will disrupt the time-frequency structure of the signal of interest after reconstruction. Lastly, spectral analysis of the reconstructed signals, such as the signal processing techniques outlined in Section 2.3, will yield results with larger uncertainties. Consider a frequency sub-band that fluctuates around the SNR limit of the lowest risk threshold. When the SNR is just above the lower limit, minor attenuation of the spectral magnitude over the corresponding frequency sub-band will be observed (up to as much as 10% of the energy). Any time the SNR drops just below the lower SNR limit, the spectral magnitude will exhibit severe attenuation (100% of the energy). The uncertainty will grow as the responses are averaged, the noise conditions shift, and transient events occur. In summary, the adaptive WPD algorithm was configured to apply the lowest risk threshold whenever the SNR drops below −5 dB (-4.4 dB accounting for uncertainty) in an attempt to preserve the integrity of the signal of interest.

5. Adaptive wavelet packet denoising algorithm implementation

The results of the simulation study were incorporated into the adaptive WPD algorithm and applied to the entire active acoustic damage detection database introduced in Section 2.2. The enhanced time responses were supplied to the signal processing techniques outlined in Section 2.3 to evaluate the enhanced damage detection performance and compare it against the performance obtained by applying a simple high pass filter. The high pass filter applied was a sixth order Butterworth filter with a cutoff frequency of 1 kHz. In both cases, data was analyzed considering only the frequency range of 1 kHz to 20 kHz due to the substantial low frequency noise contributions from the ambient environment and transient noise events (e.g. airplane pass-by noise).

5.1. Wavelet enhanced results

The data corresponding to a single test case and microphone are presented to generalize the enhancements observed across the entire database by applying the adaptive WPD algorithm. Test case L1 (edge split implemented 7.6 m down from the root) and Mic 5 (22.9 m from the root and 7.6 m from the surface) were selected and the results obtained using each signal conditioning approach are compared in Fig. 13. Specifically, two example time responses (Fig. 13a), the average band power differences (Fig. 13b), and the SAD distributions (Fig. 13c) are presented.

The time responses shown in Fig. 13a correspond to two consecutive chirp excitations measured when the blade was undamaged (D0) and exposed to a 40.6 cm long crack, the maximum level of damage (D5). Regardless of the level of severity, both time responses conditioned with the adaptive WPD algorithm exhibited a significant reduction in the ambient noise across all time and the underlying burst chirp signal was more easily distinguishable. Furthermore, the ambient noise during damage level D0 increased in amplitude (power) during damage level D5 and was still successfully removed. Lastly, a transient event in damage level D5 around 2 s was still present after spectral filtering, but removed entirely after wavelet filtering.

Considering the average band power differences (Fig. 13b), transient low frequency noise between 1 and 5 kHz during damage level D1 and D2 remained after spectral filtering but was removed when the WPD algorithm was used. The magnitudes of the average band power differences were larger after WPD due to the reduction in noise floor and enhanced ability to distinguish the chirp signal from all other noise.

The SAD distributions in Fig. 13c are shown as histograms overlaid with a normally distributed curve computed from the SAD values grouped by damage severity level. The vertical triangular line in each plot represents the damage detection threshold corresponding to three standard deviations above the mean of the undamaged SAD data set. All damage distributions to the right of the threshold were considered to be damage. When the spectral filter was used to condition the signals, the only damage that could be detected was damage level D5. Furthermore, the undamaged (D0) distribution exhibited sig-

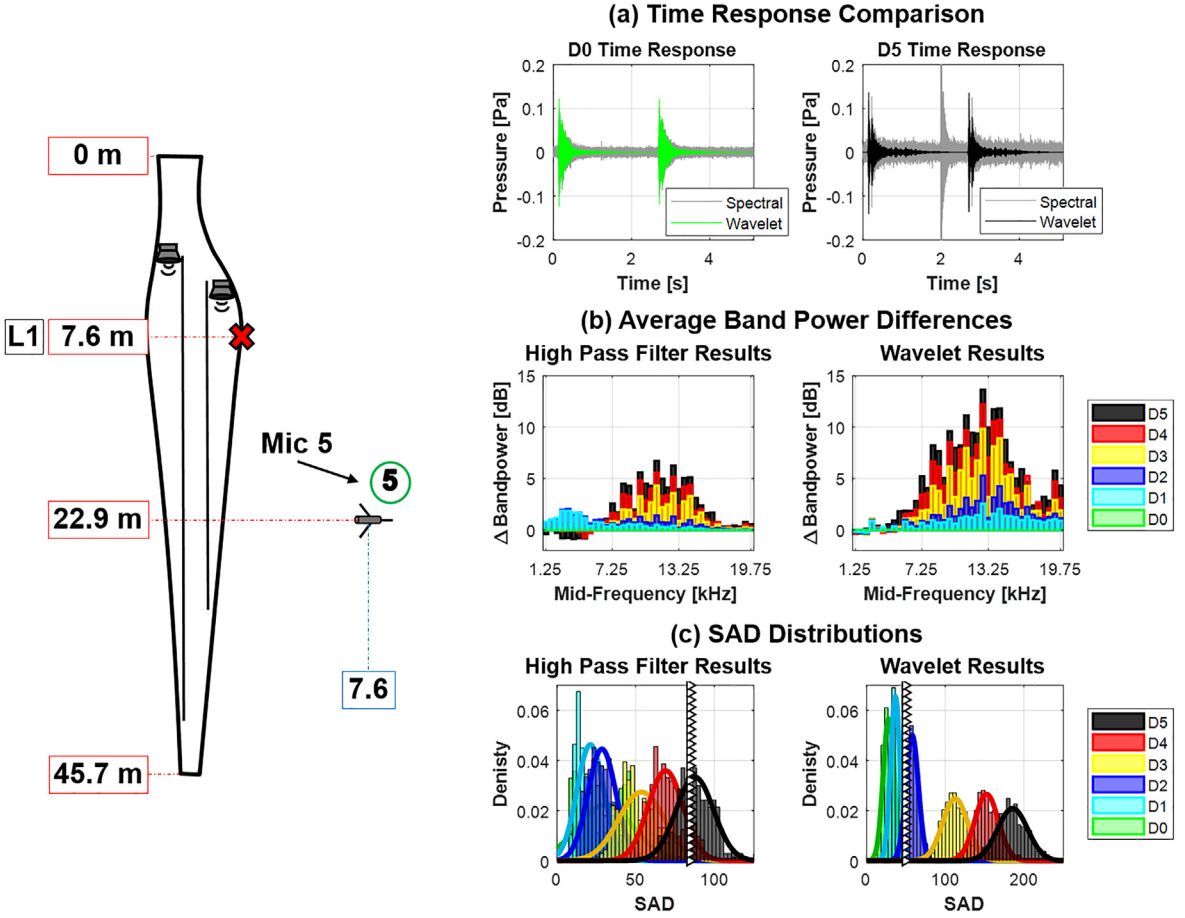

Fig. 13. Comparison of the results obtained using a high pass filter and the adaptive WPD algorithm on the data acquired from Mic 5 during test case L1. The results include: (a) undamaged (D0) and maximally damaged (D5) time responses, (b) average band power differences, and (c) SAD distributions with a damage detection threshold established as three standard deviations above the mean of the undamaged SAD dataset.

Fig. 14. Comparison of the overall damage detection performance obtained using a high pass filter and the adaptive WPD algorithm with respect to damage location.

nificant variance spreading over the SAD distributions for damage levels D1–D4. When using the adaptive WPD algorithm, the undamaged SAD distribution exhibited far less variance and damage as low as severity level D2 was easily detected.

5.2. Wavelet enhanced damage detection performance

The overall damage detection performance of the active damage detection approach was determined by recording the number of instances the mean SAD of the damage datasets (D1–D5) exceeded the damage detection threshold (three standard deviations above the mean of the undamaged data set for the respective test case and microphone). The resultant damage detection performance is shown in Fig. 14 with respect to damage location. The performance obtained when the high pass filter and WPD algorithm were used are shown in the left and right tables, respectively. The change in detection rate from the spectral filtered results to the wavelet enhanced results is identified for each location and microphone. Considering the damage detection performance with respect to location, almost all instances exhibited an improvement. Most notably was L1, in which a 60% increase was observed in the damage detection rate to a total of 84%. Test case L4 was the only location that exhibited a decrease in the detection rate. However, this was due to the reduction in false detections. Several unavoidable transient events contaminated the data acquired in test case L4 including truck engine idle noise, chain clanking, car horn honking, and airplane pass-by noise. The additional spectral content contributed by the transient events pushed the mean SAD of a few damage data sets above the damage detection threshold. Damage detected in this manner was due to the transient events and not the damage-induced differences in acoustic transmissibility. Even though damage existed during the time of measurement, the detection resulted from information completely unrelated to the damage and is undesired. Therefore, the WPD algorithm reduced the sensitivity of the damage detection performance to transient noise in the measurement.

5.3. Practical considerations

In regards to this work, several assumptions were made in the study that must be considered when implementing both the acoustics-based SHM approach and the adaptive WPD algorithm on a utility-scale wind turbine blade. First, the blade that was tested was completely stationary. In reality, the blade will be mounted to the nacelle of a wind tower and rotate as the turbine operates. Several complications will arise in regards to the interval dependency of the adaptive WPD algorithm and the acoustic propagation when applying the active damage detection approach. The time of arrival of the excitation signal will change as the relative position of the blade differs during operation. Furthermore, the time-frequency structure will no longer be linear due to Doppler shifts from the non-stationary blade when excitation is provided. In order to combat these issues, new algorithms will be needed to accurately quantify the time of arrival and signal intervals. Despite these potentially minor limitations, the active acoustic damage detection approach was applied to a 46 m utility-scale wind turbine blade and the damage detection performance was enhanced significantly using the adaptive WPD algorithm.

6. Conclusions

The need for efficient signal denoising in SHM, the potential of WPD as a solution, and the limiting assumptions of the traditional algorithm were identified. Three non-traditional approaches consisting of node-dependent noise estimation,

interval dependent thresholding, and SNR dependent threshold selection were implemented to accommodate the severe noise conditions inherent to many operational SHM environments, such as wind turbines. In order to appropriately parameterize the algorithm for denoising in operational SHM environments, a simulation study was defined that considers the tradeoff between the energy preserved corresponding to the signal of interest and the improvement to the SNR. The procedure of the simulation study was outlined such that it can be replicated for a broad range of SHM technologies, such as vibration and acoustic emission.

An active acoustic damage detection study applied to a 46 m wind turbine blade from previous work was introduced and considered as a candidate operational SHM dataset for evaluating the performance of the proposed adaptive WPD algorithm. The simulation study considering the burst chirp excitation signal used in the active acoustic damage detection tests identified the most appropriate parameters to use (wavelet function (db35), decomposition level (7), and thresholds ($T_{BM}(5)$,. . .,$T_{BM}(1)$) depending on the SNR (0.4 dB,. . .,−3.5 dB) of the measured response). The appropriately parameterized adaptive WPD algorithm was applied to the active acoustic damage detection dataset and compared with the results obtained by using a high pass filter. It was observed that the adaptive WPD algorithm could efficiently remove both ambient noise and transient noise from the measured time responses that the high pass filter was incapable of accomplishing. The enhanced time responses yielded larger band power differences and less variance when distinguishing between damage states using the considered SAD damage detection feature. The overall damage detection performance was enhanced significantly using the adaptive WPD algorithm in place of the high pass filter. A 60% improvement in the detection rate was observed from test case L1 and a reduction in the amount of false detections was observed in test case L4. The enhanced results obtained further demonstrates the capability of the acoustics-based SHM technique as a solution for wind turbine blade condition monitoring. Similar enhancements in the results and damage detection performance of other SHM technologies are expected if the adaptive WPD algorithm is considered.

CRediT authorship contribution statement

Christopher Beale: Conceptualization, Methodology, Software, Writing - original draft. **Christopher Niezrecki:** Investigation, Writing - review & editing. **Murat Inalpolat:** Supervision, Writing - review & editing, Methodology, Funding acquisition.

Declaration of Competing Interest

The authors declare that they have no known competing financial interests or personal relationships that could have appeared to influence the work reported in this paper.

Acknowledgements

This material is based upon work partially supported by the National Science Foundation under grant number 1538100 (acoustics-based structural health monitoring of closed-cavities and its application to wind turbine blades), grant number IIP-1362022 (Collaborative Research: I/UCRC for Wind Energy, Science, Technology, and Research), the Massachusetts Clean Energy Center under grant number 23576 (Development of an Integral Off-Shore Wind Turbine Blade Structural Health Monitoring System), and from the WindSTAR I/UCRC Members: Aquanis, Inc., EDP Renewables, Bachmann Electronic Corp., GE Energy, Huntsman, Hexion, Leeward Asset Management, LLC, Pattern Energy, Texas Tower Co., and TPI Composites Inc. Any opinions, findings, and conclusions or recommendations expressed in this material are those of the author(s) and do not necessarily reflect the views of the National Science Foundation, the Massachusetts Clean Energy Center or the sponsors. The authors are also indebted to Wind Technology and Testing Center (WTTC) for utilizing the utility-scale blade throughout the testing effort.

References

[1] GWEC, Global Wind Report 2017–Annual Market Update, 2018.
[2] C. Moné, M. Hand, M. Bolinger, J. Rand, D. Heimiller, J. Ho, 2015 Cost of Wind Energy Review (2017).
[3] Z. Jose, D. Michael, G. Patrick, S. Ananthan, E. Lantz, J. Cotrell, F. Beck, R. Tusing, Enabling Wind Power Nationwide, U.S. Department of Energy, United States, 2015.
[4] S. Sheng, Report on wind turbine subsystem reliability—A survey of various databases, National renewable energy laboratory-NREL/PR-5000-59111, 2013.
[5] V.A. Hines, A.B. Ogilvie, C.R. Bond, Continuous reliability enhancement for wind (crew) database: Wind plant reliability benchmark, Sandia National Laboratories: Albuquerque, NM, USA, 2013.
[6] P. Gilman, B. Maurer, L. Feinberg, A. Duerr, L. Peterson, W. Musial, P. Beiter, J. Golladay, J. Stromberg, I. Johnson, D. Boren, A. Moore, National Offshore Wind Strategy: Facilitating the Development of the Offshore Wind Industry in the United States, National Renewable Energy Lab (NREL), US, 2016, pp. 84.
[7] C.C. Ciang, J.R. Lee, H.J. Bang, Structural health monitoring for a wind turbine system: a review of damage detection methods, Meas. Sci. Technol. 19 (2008).
[8] C. Niezrecki, M. Inalpolat, Structural health monitoring of wind turbine blades using wireless acoustic sensing, US, 2015.
[9] S.N. Ganeriwala, J. Yang, M. Richardson, Using modal analysis for detecting cracks in wind turbine blades, J. Sound Vib. 45 (2011) 10–13.
[10] D. Tcherniak, Rotor anisotropy as a blade damage indicator for wind turbine structural health monitoring systems, Mech. Syst. Sig. Process. 74 (2016) 183–198.

[11] M.A. Rumsey, J.A. Paquette, Structural health monitoring of wind turbine blades, SPIE Smart Structures and Materials + Nondestructive Evaluation and Health Monitoring, SPIE, California, US, 2008, pp. 69330E-69330E-69315.
[12] P.A. Joosse, M.J. Blanch, A.G. Dutton, D.A. Kouroussis, T.P. Philippidis, P.S. Vionis, Acoustic emission monitoring of small wind turbine blades, J. Sol. Energy Eng. 124 (2002) 446–454.
[13] C. Niezrecki, P. Avitabile, J. Chen, J. Sherwood, T. Lundstrom, B. LeBlanc, S. Hughes, M. Desmond, A. Beattie, M. Rumsey, S.M. Klute, R. Pedrazzani, R. Werlink, J. Newman, Inspection and monitoring of wind turbine blade-embedded wave defects during fatigue testing, Struct. Health Monit. 13 (2014) 629–643.
[14] A. Dutton, Thermoelastic stress measurement and acoustic emission monitoring in wind turbine blade testing, European Wind Energy Conference, London (2004) 22–25.
[15] R.J.H. Paynter, A.G. Dutton, The use of a second harmonic correlation to detect damage in composite structures using thermoelastic stress measurements, Strain 39 (2003) 73–78.
[16] S. Hwang, Y.-K. An, H. Sohn, Continuous line laser thermography for damage imaging of rotating wind turbine blades, Proc. Eng. 188 (2017) 225–232.
[17] J.W. Newman, System and Method for Ground Based Inspection of Wind Turbine Blades, Digital Wind Systems, Inc., 2017.
[18] K. Lee, A. Aihara, G. Puntsagdash, T. Kawaguchi, H. Sakamoto, M. Okuma, Feasibility study on a strain based deflection monitoring system for wind turbine blades, Mech. Syst. Sig. Process. 82 (2017) 117–129.
[19] J.R. Lee, J. Takatsubo, N. Toyama, K. Dong Hoon, Health monitoring of complex curved structures using an ultrasonic wavefield propagation imaging system, Meas. Sci. Technol. 18 (2007) 3816.
[20] B. Park, Y.K. An, H. Sohn, Visualization of hidden delamination and debonding in composites through noncontact laser ultrasonic scanning, Compos. Sci. Technol. 100 (2014) 10–18.
[21] J. Sierra-Pérez, M.A. Torres-Arredondo, A. Güemes, Damage and nonlinearities detection in wind turbine blades based on strain field pattern recognition. FBGs, OBR and strain gauges comparison, Compos. Struct. 135 (2016) 156–166.
[22] M. Ozbek, D.J. Rixen, O. Erne, G. Sanow, Feasibility of monitoring large wind turbines using photogrammetry, Energy 35 (2010) 4802–4811.
[23] J. Baqersad, C. Niezrecki, P. Avitabile, Predicting full-field dynamic strain on a three-bladed wind turbine using three dimensional point tracking and expansion techniques, SPIE Smart Structures and Materials + Nondestructive Evaluation and Health Monitoring, SPIE, California, US, 2014, pp. 90612P-90612P-90613.
[24] P. Poozesh, J. Baqersad, C. Niezrecki, P. Avitabile, E. Harvey, R. Yarala, Large-area photogrammetry based testing of wind turbine blades, Mech. Syst. Sig. Process. 86 (2017) 98–115.
[25] W. Yang, Testing and Condition Monitoring of Composite Wind Turbine Blades, in: B. Attaf (Ed.), Recent Advances in Composite Materials for Wind Turbines Blades, The World Academic Publishing Co., Ltd., Hong Kong, 2013, pp. 147–169.
[26] D. Li, S.C.M. Ho, G. Song, L. Ren, H. Li, A review of damage detection methods for wind turbine blades, Smart Mater. Struct. 24 (2015) 033001.
[27] W. Yang, Z. Peng, K. Wei, W. Tian, Structural health monitoring of composite wind turbine blades: challenges, issues and potential solutions, IET Renew. Power Gener. 11 (2016) 411–416.
[28] F.P. García Márquez, A.M. Tobias, J.M. Pinar Pérez, M. Papaelias, Condition monitoring of wind turbines: techniques and methods, Renewable Energy 46 (2012) 169–178.
[29] M.A. Rumsey, An Evaluation of Sensing Technologies in a Wind Turbine Blade: Some Issues Challenges and Lessons-Learned, Sandia National Lab. (SNL-NM), Albuquerque, NM (United States), 2011.
[30] R.C. Ramachandran, G. Raman, R.P. Dougherty, Wind turbine noise measurement using a compact microphone array with advanced deconvolution algorithms, J. Sound Vib. 333 (2014) 3058–3080.
[31] D.L. Fugal, Conceptual Wavelets in Digital Signal Processing 174, Space and Signals Technical Publishing, San Diego, CA, 2009.
[32] S. Mallat, A Wavelet Tour of Signal Processing: The Sparse Way, Academic Press, 2008.
[33] R.J. Barsanti Jr, Denoising of Ocean Acoustic Signals using Wavelet-Based Techniques, Naval Postgraduate School, Monterey, CA, 1996.
[34] B.M. Gur, C. Niezrecki, Autocorrelation based denoising of manatee vocalizations using the undecimated discrete wavelet transform, J. Acoust. Soc. Am. 122 (2007) 188–199.
[35] M.B. Gur, C. Niezrecki, A wavelet packet adaptive filtering algorithm for enhancing manatee vocalizations, J. Acoust. Soc. Am. 129 (2011) 2059–2067.
[36] M.B. Gur, C. Niezrecki, A source separation approach to enhancing marine mammal vocalizations, J. Acoust. Soc. Am. 126 (2009) 3062–3070.
[37] X. Jiang, H. Adeli, Wavelet packet-autocorrelation function method for traffic flow pattern analysis, Comput.-Aided Civ. Infrastruct. Eng. 19 (2004) 324–337.
[38] M.M.R. Taha, A. Noureldin, J.L. Lucero, T.J. Baca, Wavelet transform for structural health monitoring: a compendium of uses and features, Struct. Health Monit. 5 (2006) 267–295.
[39] C. Beale, M. Inalpolat, C. Niezrecki, Active acoustic damage detection of structural cavities using internal acoustic excitations, Struct. Health Monit. (2018), Manuscript ID: SHM-18-0318, Accepted for publication.
[40] R. Canturk, M. Inalpolat, A computational acoustic interrogation of wind turbine blades with damage, Comsol Conference, Boston, MA, Oct, 2015, pp. 7–9.
[41] C. Beale, M. Inalpolat, C. Niezrecki, D.J. Willis, An experimental investigation into the insertion loss from subscale acoustic enclosures with geometric imperfections, J. Acoust. Soc. Am. 141 (2017) 3576–3577.
[42] C. Beale, M. Inalpolat, C. Niezrecki, An Experimental Investigation into the Interactions between Acoustic Modes and Structural Damage on a Cavity Structure, Proceedings of 36th International Modal Analysis Conference, Orlando, Florida, 2018.
[43] T. Regan, C. Beale, M. Inalpolat, Wind turbine blade damage detection using supervised machine learning algorithms, J. Vib. Acoust. 139 (2017), 061010-061010-061014.
[44] J. Galiana-Merino, J. Rosa-Herranz, J. Giner, S. Molina, F. Botella, De-noising of short-period seismograms by wavelet packet transform, Bull. Seismol. Soc. Am. 93 (2003) 2554–2562.
[45] S. Chang, Y.-H. Kwon, S.-i. Yang, I.-j. Kim, Speech enhancement for non-stationary noise environment by adaptive wavelet packet, Acoustics, Speech, and Signal Processing (ICASSP), 2002 IEEE International Conference on, IEEE, 2002, pp. I-561–I-564.
[46] Y. Ghanbari, M.R. Karami-Mollaei, A new approach for speech enhancement based on the adaptive thresholding of the wavelet packets, Speech Commun. 48 (2006) 927–940.
[47] J.W. Seok, K.S. Bae, Speech enhancement with reduction of noise components in the wavelet domain, Acoustics, Speech, and Signal Processing, 1997. ICASSP-97., 1997 IEEE International Conference on, IEEE, 1997, pp. 1323–1326.
[48] I.-J. Kim, S.-I. Yang, Y. Kwon, Speech enhancement using adaptive wavelet shrinkage, Industrial Electronics, 2001. Proceedings. ISIE 2001. IEEE International Symposium on, IEEE, 2001, pp. 501–504.
[49] Q. Zhang, R. Aliaga-Rossel, P. Choi, Denoising of gamma-ray signals by interval-dependent thresholds of wavelet analysis, Meas. Sci. Technol. 17 (2006) 731.
[50] M. Kharrat, E. Ramasso, V. Placet, M. Boubakar, A signal processing approach for enhanced acoustic emission data analysis in high activity systems: application to organic matrix composites, Mech. Syst. Sig. Process. 70 (2016) 1038–1055.
[51] X. Jiang, S. Mahadevan, H. Adeli, Bayesian wavelet packet denoising for structural system identification, Struct. Control Health Monitor. 14 (2007) 333–356.
[52] A. Medda, E. Chicken, V. DeBrunner, Sigma-sampling wavelet denoising for structural health monitoring, Statistical Signal Processing, 2007. SSP'07. IEEE/SP 14th Workshop on, IEEE, 2007, pp. 119–122.
[53] X. Jiang, S. Mahadevan, Bayesian wavelet methodology for structural damage detection, Struct. Control Health Monitor. 15 (2008) 974–991.

[54] M.S. Sadooghi, S.E. Khadem, A new performance evaluation scheme for jet engine vibration signal denoising, Mech. Syst. Sig. Process. 76 (2016) 201–212.
[55] MATLAB R2017, The MathWorks Inc., Natick, Massachusetts.
[56] A. Ambardar, Analog and Digital Signal Processing, Brooks/Cole Publishing Company, 1999.
[57] D.B. Percival, A.T. Walden, Wavelet Methods for Time Series Analysis, Cambridge University Press, 2006.
[58] M.V. Wickerhauser, Adapted Wavelet Analysis: From Theory to Software, AK Peters/CRC Press, 1996.
[59] D.L. Donoho, J.M. Johnstone, Ideal spatial adaptation by wavelet shrinkage, Biometrika 81 (1994) 425–455.
[60] M. Misiti, Y. Misiti, G. Oppenheim, J.-M. Poggi, Wavelet Toolbox User's Guide, The MathWorks Inc., Natick, MA, 1996.
[61] RSG, Massachusetts Study on Wind Turbine Acoustics, 2016.
[62] L. Birgé, P. Massart, From model selection to adaptive estimation, Festschrift for lucien le cam, Springer, 1997, pp. 55–87.
[63] A. Barron, L. Birgé, P. Massart, Risk bounds for model selection via penalization, Probab. Theory Relat. Fields 113 (1999) 301–413.
[64] G. Luo, D. Zhang, Wavelet Denoising, Advances in Wavelet Theory and Their Applications in Engineering, Physics and Technology, InTech, 2012, pp. 59–80.
[65] E. Burhan, Signal and Image Denoising Using Wavelet Transform, Advances in Wavelet Theory and Their Applications in Engineering, Physics and Technology, InTech, 2012, pp. 495–514.
[66] Y. Feng, F.S. Schlindwein, Normalized wavelet packets quantifiers for condition monitoring, Mech. Syst. Sig. Process. 23 (2009) 712–723.